Article

Journal of Vibration and Control
1–17

DOI: 10.1177/1077546317693432
journals.sagepub.com/home/jvc
SAGE

Road excitation classification for semi-active suspension system based on system response

Yechen Qin, Changle Xiang, Zhenfeng Wang and Mingming Dong

Abstract

Vehicle performance is largely affected by the properties of the suspension system, where semi-active suspension has been widely used in mass production of vehicles owing to its characteristics such as internal stability and low energy consumption. To solve the contradiction between ride comfort and road handling, road estimation based semi-active suspension has received considerable attention in recent years. In order to provide accurate estimation for advanced control strategies applications, this paper aims to develop a new method that can provide precise road class estimation based on measurable suspension system response (i.e. sprung mass acceleration, unsprung mass acceleration and rattle space). The response signal is first decomposed using wavelet packet analysis, and features in both time and frequency domains are subsequently extracted. Then, minimum redundancy maximum relevance (mRMR) is utilized to select superior features. Finally, a probabilistic neural network (PNN) classifier is applied to determine road classification output. The most representative semi-active control strategy, i.e. skyhook control, is used to validate this method, and simulation results with varying conditions including different control parameters and sprung mass are compared. The results show that unsprung mass acceleration is most suitable for road classification, and more robust to varying conditions in comparison to other responses.

Keywords

Adaptive suspension system, minimum redundancy maximum relevance (mRMR), road estimation, semi-active suspension system, wavelet packet analysis

1. Introduction

Recent developments in automotive technology have resulted in an increasing market demand for improving drivers' comfort; however, for current widely used passive suspension systems, this cannot be achieved without sacrificing road handling capabilities (Hrovat, 1997; Rath et al., 2016; Zhao, 2016). To remedy this, semi-active suspension systems have emerged as a viable option, and have been successfully used in mass production of vehicles (Savaresi et al., 2010). In comparison to active suspension systems, semi-active suspension has been demonstrated to have similar performance in terms of ride comfort (Yi and Song, 1999). In addition, semi-active suspensions have the potential advantage of improving internal stability, lowering energy costs and dispensing with extra power resource. All these advantages have made semi-active suspension systems a major focus of research in recent years (BalaMurugan and Jancirani, 2012; Poussot et al., Qin et al., 2015a, 2015b). Most of contemporary research mainly focuses on improving control strategies' performance by choosing only one or few control parameters or by assuming that driving conditions remain unchanged while driving (Liu et al., 2008; Sankaranarayanan et al., 2008; Ahmed and Svaricek, 2014).

School of Mechanical Engineering, Beijing Institute of Technology, People's Republic of China

Received: 7 October 2016; accepted: 4 January 2017

Corresponding author:
Mingming Dong, School of Mechanical Engineering, Beijing Institute of Technology, 100081, Beijing, People's Republic of China.
Email: vdmm@bit.edu.cn

Unfortunately, such assumptions are not valid in practical applications. First, it has been observed that the contradiction between ride comfort and road handling still exists in semi-active suspension system, and suspension's performance is completely determined by the choice of control parameters or gains (Qin et al., 2016). Second, the unchanged driving conditions assumption is impractical in real-world situations as the sprung mass and road conditions are known to have significant variation. Under these circumstances, a major problem in design of semi-active suspension systems is related to the choice of control parameters or gains for varying road conditions. To address this particular problem, adaptive suspension systems for varying road conditions with the gain tuning principle given by Hong et al. (2002) have been proposed and have received considerable attention (Qin et al., 2015a; Turnip and Hong, 2013; Zhang et al., 2012). In this case, the estimation of road conditions is critical for commercial applications of semi-active suspension systems.

Current road estimation methods can be divided into three categories (Qin et al., 2014): direct measurements (Doumiati et al., 2011; Imine et al., 2006), noncontact measurements (McCann and Nguyen, 2007) and system response based estimation (Nordberg, 2004; Rabhi et al., 2006; Gonzalez et al., 2008; Koch et al., 2010; Qin et al., 2012, 2015b). Among these three categories, the first two require specific instruments designs, which restrict their practical applications. Depending on sensors that were originally designed for system control, the last method is often used to estimate road excitation, and estimated results (i.e. the road level) can be further applied to adaptively change control parameters or gains (Turnip and Hong, 2013; Ahmed and Svaricek, 2014).

Research related to the estimation of the road level has been carried out in either time or frequency domains (Hong et al., 2002; Gonzalez et al., 2008; Zhang et al., 2012; Yu et al., 2013; Qin et al., 2015b). However, previous research either is only applicable for passive suspension systems (Imine et al., 2006; Ngwangwa et al., 2014), or depends on system variables that cannot be directly measured (Nordberg, 2004; Martinez et al., 2015). Moreover, detailed analysis related to the relationship between semi-active suspension system responses and time and\or frequency domain features in the aspect of road classification has not been done, and the performance of road estimation algorithms for varying driving conditions has not been fully investigated.

In this paper, a novel method to classify road levels based on measurable system response signals is proposed, which overcomes the problems mentioned above. Measurable signals for the suspension system, including the sprung mass acceleration, unsprung mass acceleration and rattle space, are treated as candidate signals. Next, the wavelet packet decomposition is carried out to obtain six components with different frequency ranges. Then, four basic statistical features, i.e. the variance, square root of amplitude (SRA), root mean square (RMS) and maximum value, are applied to generate 29 features for each candidate signal. To avoid high dimensionality, the four most superior features are selected using the minimum redundancy maximum relevance (mRMR). Finally, a probabilistic neural network (PNN) classifier is applied to determine the road class.

The novel contributions of the paper are as follows.

- First, a new road classification method is developed by combing information available from both time and frequency domains. This is different from previous methods, as features in different frequency ranges are fully investigated and utilized. The selection of superior features proposed in this paper can depress influence caused by control strategies, improving classification accuracy, and avoid problems associated with higher dimensional spaces.
- Second, the classification accuracy and robustness of the proposed method are compared to existing methods with varying driving conditions. Simulation results demonstrate the superiority and improved robustness of the proposed method.
- Finally, contrary to previous studies, the proposed method can accurately estimate varying road excitation of different frequency structures, which makes it more suitable for practical applications.

In this paper, concepts such as the system models of quarter of vehicle (QoV), skyhook control strategy and road profile are first introduced. This is followed by defining 29 features in both time and frequency domains, which are used to estimate candidate signals, and generated using basic statistical features. Next, the procedures of the proposed method, including signal pre-processing, feature fusion, feature reduction and classification with the PNN, are described. Finally, the results for varying driving conditions for three response signals are discussed.

2. System model

2.1. Quarter of vehicle (QoV) model

The QoV model including damping characteristics and skyhook control strategy are discussed in this section. Owing to its simplicity, the QoV model has been widely accepted as a system model in the field of

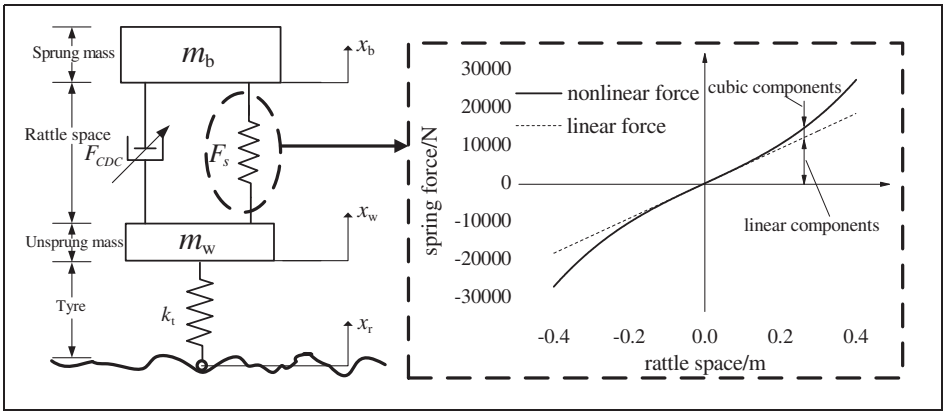

Figure 1. Quarter of vehicle (QoV) model.

suspension control. The structure of a nonlinear QoV model is shown in Figure 1.

The dynamic equations of the QoV model are given by equation (1)

$$\begin{aligned} m_{\mathrm{b}}\ddot{x}_{\mathrm{b}} + F_s + F_{CDC} &= 0 \\ m_{\mathrm{w}}\ddot{x}_{\mathrm{w}} + k_{\mathrm{t}}(x_{\mathrm{w}} - x_{\mathrm{r}}) - F_s - F_{CDC} &= 0 \end{aligned} \tag{1}$$

where, x_{b}, $\dot{x}_{\mathrm{b}}$ and $\ddot{x}_{\mathrm{b}}$ are the displacement, velocity and acceleration of the sprung mass, respectively, x_{w}, $\dot{x}_{\mathrm{w}}$ and $\ddot{x}_{\mathrm{w}}$ are the displacement, velocity and acceleration of the unsprung mass, respectively, x_{r} is road unevenness, F_{CDC} is damping force generated from the continuous damping control (CDC) damper, and F_s is the nonlinear spring force. The relationship between the rattle space (the distance between the sprung mass and unsprung mass) and spring force can be expressed by the following cubic equation

$$F_{ks} = k_s(x_b - x_w) + \varepsilon k_s(x_b - x_w)^3 \tag{2}$$

where ε is the cubic coefficient, and k_s stands for linear spring stiffness.

In this paper, in order to validate the proposed classification method, skyhook control is applied to generate the control force F_{CDC}. Since it was first proposed in 1970s (Karnopp et al., 1974), skyhook control has been widely utilized as a reference control strategy in the field of semi-active suspension. To mimic the behavior of an ideal skyhook model, the following control rules need to be satisfied

$$F_{\mathrm{sky}} = \begin{cases} c_{\mathrm{sky}}(\dot{x}_{\mathrm{b}}), & \text{if } (\dot{x}_{\mathrm{b}} - \dot{x}_{\mathrm{w}}) \cdot \dot{x}_{\mathrm{b}} \geq 0 \\ c_{\mathrm{min}}(\dot{x}_{\mathrm{b}} - \dot{x}_{\mathrm{w}}), & \text{if } (\dot{x}_{\mathrm{b}} - \dot{x}_{\mathrm{w}}) \cdot \dot{x}_{\mathrm{b}} < 0 \end{cases} \tag{3}$$

$$F_{CDC} = \mathrm{sat}\{F_{\mathrm{sky}}\} \tag{4}$$

where sat represents the saturation of the damper force.

A CDC damper from ZF Sachs is used in this paper. A photograph of a strut with the selected CDC damper and coil spring is shown in Figure 2(a). The dynamic characteristics of the CDC damper are tested using an MTS load frame. The load frame with the mounted damper is shown in Figure 2(b). The force and displacement are measured using a load cell and linear variable differential transformer (LVDT) sensor. The control current varies from 0A to 1.8A with increments of 0.2A. The velocity-force map for the adopted CDC damper is shown in Figure 2(c).

The parameters of the quarter vehicle model are listed in Table 1.

2.2. Road profile model

In this part, the characteristics of six representative road levels and their time domain realization are discussed.

The distance between the base plate and road surface is defined as a function of road irregularities $Q(i)$, where i is the distance along the path. In this paper, assumption 1 is tenable.

Assumption 1. Road profile is a homogeneous and isotropic Gaussian random process.

With assumption 1, the statistical characteristics of the road profile can be approximately expressed by equation (5)

$$G_q(n) = C_{sp} n^{-W} \tag{5}$$

where $G_q(n)$ is the power spectral density (PSD) of the road profile, n is the spatial frequency in m^{-1}, C_{sp} and W are two constants representing the excitation energy and PSD slope, respectively. The values of these two constant parameters for different road types are tabulated in Table 2 (Deusen, 1968; ISO, 1995; Wong, 2001)

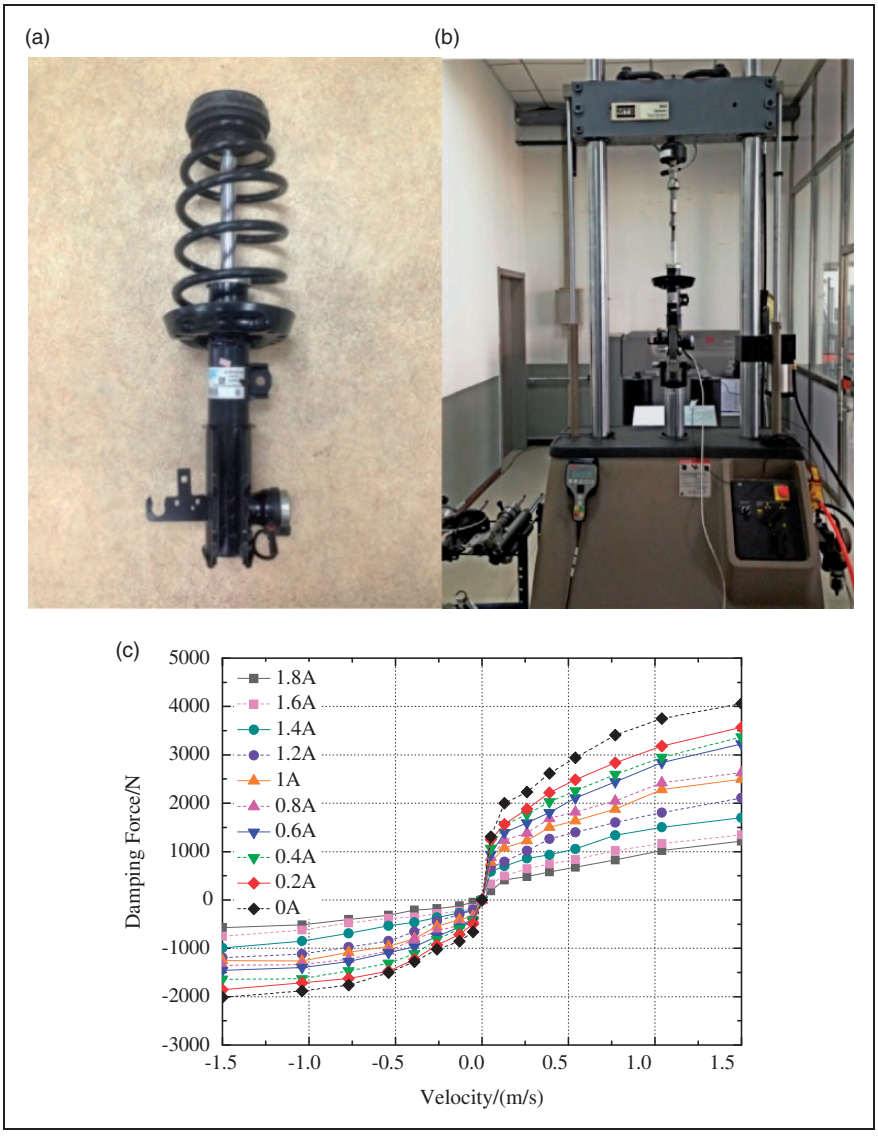

Figure 2. (a) Image of strut with CDC damper and coil spring; (b) Damper mounted in MTS load frame; (c) Velocity-force map for CDC damper.

Table 1. Parameters of quarter of vehicle model (QoV).

Symbol	Description	Value
m_b	Sprung mass	410 kg
m_w	Unsprung mass	39 kg
k_t	Tire spring stiffness	183,000 N/m
k_s	Suspension spring stiffness	20,000 N/m
ε	Nonlinear stiffness coefficient	3

Table 2. Parameters for six representative road types.

No.	Description	W	C_{sp}
1	Smooth Runway (SR)	3.8	4.3×10^{-11}
2	Smooth Highway (SH)	2.6	1.9×10^{-8}
3	ISO-Level B (ISO-B)	2	6.4×10^{-7}
4	Highway with Gravel (HG)	2.1	4.4×10^{-6}
5	ISO-Level E (ISO-E)	2	4.1×10^{-5}
6	Pasture (PA)	1.6	3×10^{-4}

and Figure 3. Abbreviations for each level are shown in parentheses.

It can be seen from Figure 3 that the six road types are of different frequency structures, and higher W lead to higher low-frequency components and lower high-frequency components, as shown in SR (smooth runway). And such kinds of varying frequency structures bring new challenges for road classification.

When a vehicle is driving with velocity v, spatial frequency n in equation (5) can be transformed into time

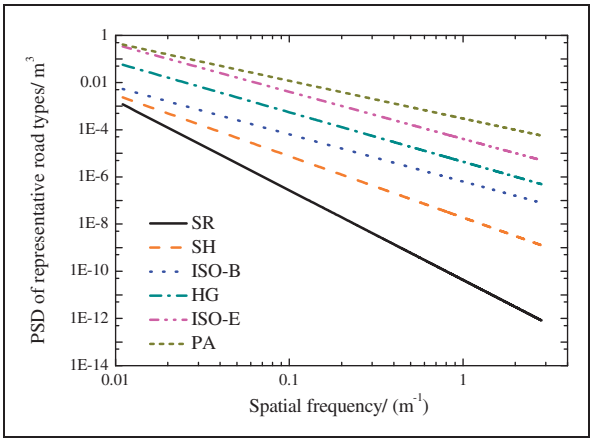

Figure 3. PSD (power spectral density) of six representative road types.

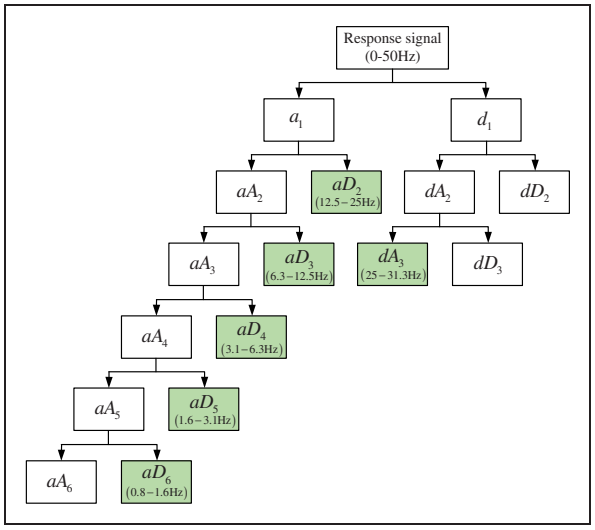

Figure 4. Structure of six-layer wavelet packet decomposition.

frequency f according to equation (6)

$$f = vn \tag{6}$$

Since all values of W in Table 2 are not equal to 2, the harmony superposition method is applied to generate the road profile in the time domain. Assuming that the frequency range of the road profile can be equally divided into M parts, harmony superposition can be expressed by equation (7) (Qin et al., 2014)

$$q(t) = \sum_{K=1}^{M} \sqrt{2 \cdot G_q(f_{\text{mid}-\text{K}}) \cdot \frac{f_2 - f_1}{M}} \sin(2\pi f_{\text{mid}-\text{K}} t + \Phi_{\text{K}}) \tag{7}$$

where $q(t)$ is the road profile in the time domain, $f_{\text{mid}-\text{K}}$ is the kth middle frequency in Hz,$G_q(f_{\text{mid}-\text{K}})$ represents the PSD of $f_{\text{mid}-\text{K}}$ in m^3, Φ_{K} represents the independent and identically distributed (IID) random phase over $(0, 2\pi)$, f_1 and f_2 are the upper and lower frequency bounds, respectively.

According to ISO8608 (ISO, 1995), the upper and lower spatial frequencies are set as $0.011\,\text{m}^{-1}$ and $2.83\,\text{m}^{-1}$. Considering the commonly used velocity range of $v = 10 \sim 30\,\text{m/s}$, f_1 and f_2 were set as 0.33 Hz and 28.3 Hz, respectively.

3. Feature definition

A total of 11 different features for salient features selection has been proposed in literature (Qin et al., 2015b). Results revealed that features related to signal energy have significantly better performance in comparison to other feature categories. In this paper, four superior features, namely, the variance, SRA, RMS and maximum value (Max.) are selected as basic statistical features. For a signal $x(n)$ of length N, the selected features are defined as follows

$$\text{Variance} = \sqrt{\frac{\sum_{n=1}^{N} (x(n) - \bar{x})^2}{N-1}},$$

$$\text{SRA} = \left(\frac{\sum_{n=1}^{N} \sqrt{|x(n)|}}{N} \right)^2,$$

$$\text{RMS} = \sqrt{\frac{\sum_{n=1}^{N} (x(n))^2}{N}}, \quad \text{Max} = \max|x(n)|$$

where $\bar{x}$ is the mean value of $x(n)$.

Since road excitation has a relatively low amplitude at low frequencies and high amplitude at high frequencies, the generated frequency response of the three candidate signals are found to be significantly different. Thus, the system response in different frequency ranges should be fully investigated. In this case, the wavelet packet decomposition technique is applied, and the structure of six level wavelet packet decompositions is shown in Figure 4.

Frequencies f_1 and f_2 are set as 0.33 Hz and 28.3 Hz according to Section 2.2. A frequency band ranging from 0.8 Hz to 31.3 Hz is applied to approximate such a frequency range. The six corresponding frequency components, i.e. aD2-aD6 and dA3, are marked in shaded boxes in Figure 4. The sampling rate is set to be 100 Hz with the analysis frequency range of $0 \sim 50$ Hz. This sampling frequency is more than sufficient for the analysis and comparison of the suspension system, which has an upper frequency bound of approximately 30 Hz.

In this paper, a total of 29 features are extracted from both time and frequency domains. The definitions of these 29 features are stated below, and index numbers of features are tabulated in Table 3.

Table 3. Index number of 29 features.

Features		Variance	SRA	RMS	Max	Energy
Time Domain		1	2	3	4	N/A
Frequency Domain	Energy	N/A	N/A	N/A	N/A	5
	aD2	6	12	18	24	N/A
	aD3	7	13	19	25	N/A
	aD4	8	14	20	26	N/A
	aD5	9	15	21	27	N/A
	aD6	10	16	22	28	N/A
	dA3	11	17	23	29	N/A

RMS: root mean square; SRA: square root of amplitude

- Four time domain features: four basic statistical features are defined as time domain features.
- Twenty-four frequency domain features: four basic statistical features are calculated for six components corresponding to frequency range of 0.8–31.3 Hz.
- One energy feature: signal energy is calculated as the sum of squared terms for six frequency components

$$Energy = \sum_{i=2}^{6} ||aD_i||^2 + ||dA_3||^2$$

4. Classification algorithm

The structure of the process for the proposed classifier applied to each candidate signal is illustrated in Figure 5. The proposed method can be divided into four stages, namely, signal sampling and pre-processing, feature fusion, feature reduction and classification. In Section 3, the definition of features (feature fusion) has been discussed. In this section, other three stages of the process are explained in detail.

4.1. Signal sampling and pre-processing

Three different system responses (i.e. the sprung mass acceleration, unsprung mass acceleration and rattle space) are selected as candidate signals for analysis. The sampling rate is set at 100 Hz. To extract features from the three candidate signals and improve classification accuracy, pre-processing of the signals is performed. The pre-processing is implemented in three distinct steps: low pass filtering, framing and windowing.

Remark 1. The pre-processing procedure is indispensable for both classifier training and validation process.

1. Low pass filtering

Here, the sampling rate and upper frequency bound are set as 100 Hz and 31.3 Hz. To avoid signal aliasing, a low pass filter with a low cut-off frequency of 50 Hz is firstly applied to the signal.

2. Framing

Assuming the classification interval as 1 s, for a 100 Hz sampling rate, it is typically hard for the controller to simultaneously achieve a high resolution for both high- and low-frequency components. To obtain sufficient information for low frequency components, the length of the frame for candidate signals is set to 200, with 100 points from the previous interval (50% overlap). Thus, 29 features can be calculated according to these 200 points per second.

3. Windowing

To prevent a spectral leak at the start and end of a frame, a Hamming window is applied, given by

$$Z(k) = 0.54 - 0.46\cos\left(2\pi\frac{k}{N-1}\right), k = 0, 1, \ldots, N-1 \tag{8}$$

where $N = 200$ is the number of points in each frame. Assuming that $x(t)$ is the signal in a frame, the output signal after windowing can be expressed as

$$y(t) = x(t) \cdot z(t) \tag{9}$$

4.2. Feature reduction

After implementing feature fusion, a total of 29 features are obtained. Here, all of the calculated 29 features can be used to perform classification; however, the dimensionality problem may deteriorate the performance of the classifier.

- Since the complexity of the classifier is largely dependent on the number of input variables, a large number of input variables leads to a significant increase in the computation time.

Another feature reduction method utilized in the authors' previous paper called "Improved distance evaluation method" has proved to be effective (Qin et al., 2015b), but since the superior features selected only depend on the relative distance, this method may suffer from data redundancy.

- It has been realized that a combination of all individual good features does not always lead to superior performance (Jain et al., 2000). In such a

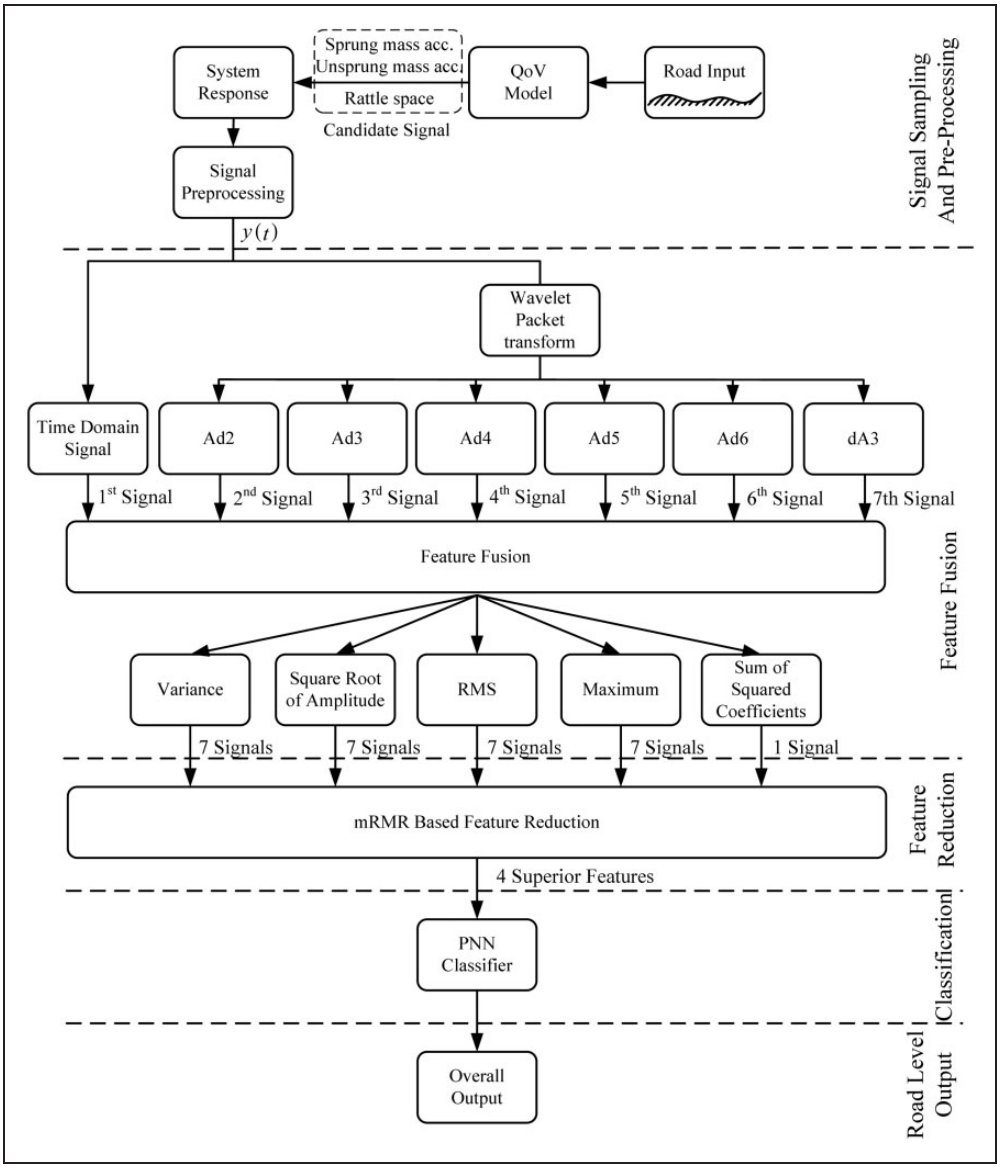

Figure 5. Flow chart of classification algorithm.
QoV: quarter of vehicle; RMS: root mean square; PNN: probabilistic neural network.

situation, a method that would allow the selection of features with minimal redundancy is required.

To solve the aforementioned problems, the mRMR method is applied to select features from the previously obtained 29 features. This method is based on the maximal relevance and minimum mutual redundancy (Ding and Peng, 2005; Peng et al., 2005).

The mRMR introduces a criterion called the mutual information (MI) to measure the relevance between two variables m and n, which is defined as follows

$$I(m,n) = \sum_{i,j} p(m_i, n_j) \log \frac{p(m_i, n_j)}{p(m_i)\, p(n_j)} \tag{10}$$

where $p(m,n)$ is the joint probabilistic distribution, and $p(m)$ $p(n)$ are the marginal probabilities of m and n, respectively. Given a signal of length M with two variables m and n, the functions of $p(m,n)$, $p(m)$ and $p(n)$ can be estimated using the Gaussian kernel estimator, as defined in the following equations (Cai et al., 2012)

$$p(m,n) = \frac{1}{M} \sum_{i=1}^{M} \frac{1}{2\pi h^2} e^{-\frac{1}{2h^2}\left[(m-m_i)^2 + (n-n_i)^2\right]} \tag{11}$$

$$p(m) = \frac{1}{M} \sum_{i=1}^{M} \frac{1}{\sqrt{2\pi h^2}} e^{-\frac{1}{2h^2}(m-m_i)^2} \tag{12}$$

$$p(n) = \frac{1}{M}\sum_{i=1}^{M}\frac{1}{\sqrt{2\pi h^2}}e^{-\frac{1}{2h^2}(n-n_i)^2} \tag{13}$$

where h is a tuning parameter used to control the width of kernels.

Assuming that feature set S is a set of minimal redundancy with a predefined features number of p, the minimum redundancy condition can be expressed by equation (14).

$$\min W_I,\ \ W_I = \frac{1}{|S|^2}\sum_{i,j\in S} I(g_i, g_j) \tag{14}$$

where $|S| = p$ is set as the feature number in S, and g_i stands for feature i.

To maximize the total relevance of all features in S, the MI of $I(h, g_i)$ between predefined target class $h = \{h_1, h_2, \ldots h_k\}$ and feature expression g_i is calculated. Then, the condition of maximum relevance can be defined as equation (15)

$$\max \mathrm{V}_I,\ \ V_I = \frac{1}{|S|^2}\sum_{i\in S} I(h, g_j) \tag{15}$$

With conditions shown in equation (14) and equation (15), the mRMR superior feature set can be obtained by simultaneously optimize both conditions. The combination of two opposite conditions into one unique criterion require two criterions (Ding and Peng, 2005)

$$\max(V_I - W_I) \tag{16}$$

$$\max(V_I / W_I) \tag{17}$$

In this paper, the criterion shown in equation (17) is applied to select superior features. The process of feature reduction is performed for all three candidate signals and in both training and validation.

4.3. PNN classifier

The PNN classifier is first proposed by Specht (1990) to solve problems related to pattern classification. With predefined features and categories, the PNN uses a training set to develop a distribution function to calculate the likelihood of features within different categories. The PNN originated from the RBFNN in combination with the Bayesian decision theory. A well-known Bayesian formula is shown in equation (18)

$$P(X|Y) = \frac{P(Y|X)P(X)}{P(Y)} \tag{18}$$

where $P(X)$ and $P(Y)$ are the known prior probabilities of events X and Y, respectively. To calculate the posterior probability of event X with event Y having already occurred ($P(X|Y)$), $P(X)$, $P(Y)$ and the posterior probability of event Y with event X having already occurred should be known. When applying the Bayesian formula for classification, event Y can be interpreted as the possibility that a pattern can be placed, and event X is interpreted as the pattern. The Bayesian theory tries to place this pattern into a category with the highest probability.

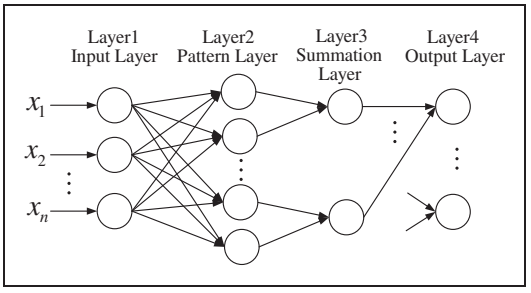

Figure 6. Structure of typical PNN (probabilistic neural network).

The structure of a typical PNN is shown in Figure 6.

A typical PNN contains four layers, where the value of the data set is imported from the input layer into the network. Neurons in the pattern layer are connected with the input layer. The number of neurons is equal to the number of patterns in the training set. The weighted sum of each neuron is calculated according to a nonlinear activation function, as shown in equation (19)

$$\Phi(I_i) = \mathrm{e}^{\frac{I_i - 1}{\sigma^2}} \tag{19}$$

where I_i is the ith weight between the input and pattern layer, and σ is a smoothing parameter. The choice of σ is discussed in detail in Specht (1990).

Neurons in the summation layer simply sum all neurons that belong to the same category in the pattern layer with unit weights. This allows the estimation of probability density for each category. After normalization in the output layer, the final output is obtained.

Remark 2. The number of outputs in the fourth layer equals the number of categories, and each output is binary, i.e. the output of the category with the largest probability is set to be 1 and is chosen as the overall output.

5. Simulation

5.1. Overall structure and simulation setting

A block diagram illustrating the proposed method is shown in Figure 7. The block diagram can be divided

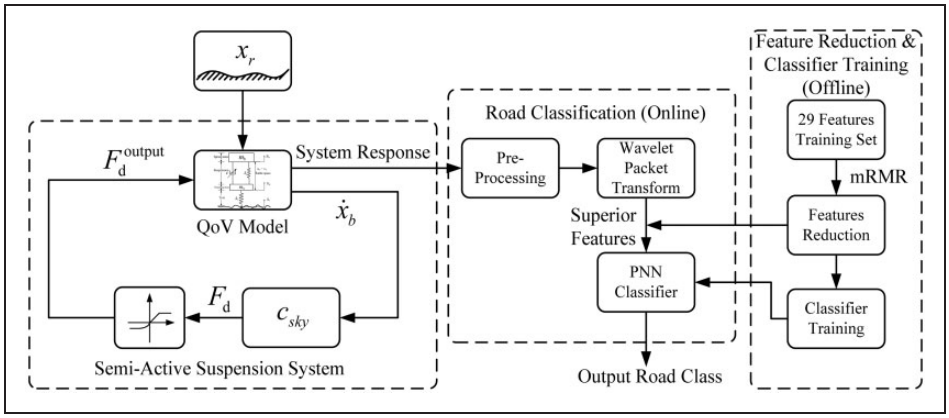

Figure 7. Block diagram representing overall estimation strategy.
QoV: quarter of vehicle; mRMR: minimum redundancy maximum relevance.

into three distinct parts: the semi-active suspension system, feature reduction & classifier training and road classification. The first part contains the QoV model and generates system responses. The second part is used to output superior features and train the PNN classifier with training data offline. The remainder portion is performed online used to identify the road class.

In the part with the semi-active suspension system, the QoV model is stimulated by road excitation, the velocity of sprung mass is used to generate the calculated control force F_d, and the controllable damping force F_d^{output} is used as the system control force after force saturation.

Remark 3. In this paper, the velocity of sprung mass $\dot{x}_b$ is assumed to be available, as the main focus of this work is on road classification, and in real-world applications, a state observer, e.g. Kalman Filter (KF), can be implemented to observe this unknown variable.

Generated system responses from the suspension system are then applied for road classification. After signal sampling and preprocessing discussed in Section 4.1, the wavelet packet transform is utilized to generate 29 features. Superior features are then imported into the PNN classifier, and the road class is identified.

For the purpose of system training and method validation, system definitions are listed in Table 4, and assumptions are provided to be tenable.

Assumption 2. The velocity of the vehicle is maintained at 40 km/h.

Assumption 3. The road level remains unchanged within each 100 s (the training process) and 50 s (the validation process) intervals.

Table 4. Definitions for training and validation process.

Term	Description
c_{sky}	1500 N s/m
c_0	300 N s/m
Classification interval	1 s
Vehicle velocity	40 km/h
Setting of training road	100 s for each class, totally 600 s
Sequence of training road	SR, SH, ISO-B, HG, ISO-E, Pasture
Setting of validation road	50 s for each class, totally 300 s
Sequence of validation road	SR, HG, ISO-B, Pasture, SH, ISO-E

Assumption 4. The translation time for two different road levels is neglected.

In order to train the PNN classifier and obtain the superior feature set, a driving period with the time duration of 600 s on a road with all six road levels is generated with the application of harmonic superposition. System responses including the three candidate signals are then generated with the QoV model and skyhook control. Using the generated system responses, 29 features for the three candidate signals are calculated. Then, the mRMR is used to derive four superior features form the superior feature set. The index numbers of superior features for each candidate signal are tabulated in Table 5.

Remark 4. The total number of features in the superior set is arbitrary, and a larger number of features implies availability of more information which can be applied for classification. However, this would also increase system complexity.

Table 5. Superior features for candidate signals.

Feature	Index number	Description	Index number	Description
Sprung mass acceleration	2	SRA of time domain	3	RMS of time domain
	12	SRA of aD2	23	SRA of dA3
Unsprung mass acceleration	2	SRA of time domain	4	Max of time domain
	20	RMS of aD4	29	Max of dA3
Rattle space	2	SRA of time domain	18	RMS of aD2
	20	RMS of aD4	23	RMS of dA3

RMS: root mean square; SRA: square root of amplitude

With selected features, three PNN classifiers are generated for the three candidate signals. Both superior feature sets and classifiers are stored for the subsequent real time application.

In order to evaluate the performance of the proposed classifier, a new validation road signal with duration of 300 s is generated. The validation results of the proposed classifier are discussed in the subsequent section.

5.2. Simulation results

Simulations are used to validate the nominal model and model with uncertainties. Uncertainties include the varying control parameter value c_{sky} and sprung mass.

5.2.1. Simulation results of nominal model. The results for the nominal model with system parameters and conditions defined in Table 1 and Table 4 are shown in Figure 8. To better illustrate the prosperity of the proposed classifier, classification errors are marked with red circles in all figures.

It can be seen from Figure 8 that for the nominal model, all three system responses can accurately identify all six road levels with accuracy of more than 86%. Compared to the rattle space, both sprung mass and unsprung mass acceleration demonstrate better performance. The lowest classification accuracy of these two responses is 94%. It can also be observed from Figure 8(a)–(c) that almost all classification errors occur when the road level changes. This error can be attributed to the framing procedure mentioned in Section 4.1, where 50% previous information is repeated. Although, the transformation time is significantly short between different road levels, and such a kind of aliasing is unavoidable. In addition, error points shown in Figure 8(a)–(c) indicate that the difference between two adjacent roads also greatly influences classification accuracy. When the difference is relatively large, errors are observed, which are related to the difference. As an example, when the road changes from a pasture to smooth highway (the difference of four levels), the classification with the sprung mass acceleration and rattle space required three intervals (3 s) to converge to a smooth highway, and the unsprung mass acceleration requires two intervals (2 s). Conversely, when the road level changes from a highway with gravel to ISO level B, no classification error occurred for the sprung mass and unsprung mass acceleration. For the rattle space, the classification results for a highway with gravel are unsatisfactory, where 14% of HG roads are incorrectly classified as ISO level B. The reason for this can be discussed in accordance with Table 2, where it can be seen that the difference between the HG and ISO level B is smaller than other classifications.

5.2.2. Simulation results of control parameter $c_{sky} = 4000$ Ns/m. In order to balance the contradiction between the ride comfort and road handling, control parameters and gains need to adaptively change with variations in the conditions of road excitation (Qin, 2016). Since, the variation of control parameters and gains influence system responses, further discussion of the parameters is needed. In this part, skyhook control parameter c_{sky} in Table 4 varies from 1500 Ns/m to 4000 Ns/m. The reason why these two parameters are chosen is that these two parameters can cover the force output capacity of the controllable damper for varying road levels. The results are shown in Figure 9.

It can be seen from Figure 9 that compared to the results of the nominal model, the change of classification results for different control parameters and gains is not obvious. This result can be interpreted as follows. Previous research has revealed that, owing to the existence of damping force saturation, although the performance of semi-active suspension systems can be adjusted, the variation range is only about 10–15% (Qin et al., 2016). Under the circumstance, changing of control parameters and gains has little effect on the classifier performance, and robustness can be ensured for this case.

5.2.3. Simulation results of sprung mass $m_b = 500$ kg and $m_b = 30$ kg. The value of the sprung mass for vehicle changes a lot according to driving conditions, where

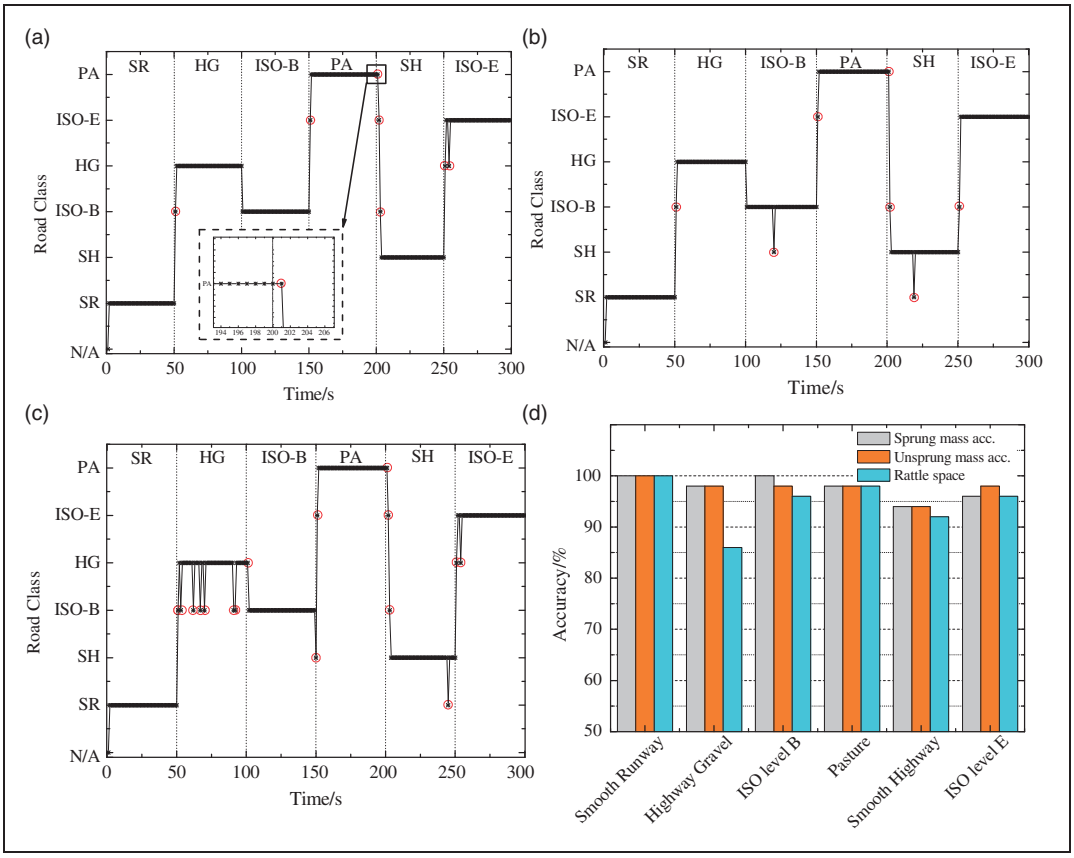

Figure 8. Classification results for nominal model: (a) sprung mass acceleration, (b) unsprung mass acceleration, (c) rattle space, (d) classification accuracy.

30% variation of the sprung mass value may appear (Liu et al., 2008). To evaluate the classifier's performance for different sprung masses, system responses with $m_b = 500\,\text{kg}$ and $m_b = 300\,\text{kg}$ are imported into the trained classifier generated in Section 5.1. The results are presented in Figure 10.

It can be seen from Figure 10 that the proposed classifier is susceptible to variations in the sprung mass. Compared to the variation of the control parameter, changes in the sprung mass deteriorate the classifier performance, especially for the sprung mass based classifier. Classification errors predominantly occurred while driving on a Highway with Gravel and ISO-E in both Figure 10(a) and (b). Among the three sensors, the sprung mass acceleration has higher sensitivity compared to the other two sensors. For the case of $m_b = 500\,\text{kg}$, the classification accuracy of both levels decreased from 98% and 96% to 76% and 84%, respectively. On the other hand, the accuracy of the unsprung mass acceleration becomes 86% and 98% from 98% and 98%, respectively. In the case $m_b = 300\,\text{kg}$, the classification accuracy of both levels change from 98% and 96% to 80% and 88%, respectively, whereas the accuracy of the unsprung mass acceleration become 86% and 98% from 98% and 98%, respectively. In this case, it can be concluded that the unsprung mass acceleration is more robust to variations in the sprung mass than the sprung mass acceleration.

5.2.4. Robustness illustration based on frequency characteristics. In order to provide additional insight into the proposed classifier, and further discuss reasons associated with the deterioration of the classification results for different conditions, frequency responses of the sprung mass acceleration, unsprung mass acceleration and rattle space are analyzed. These results are shown in Figures 11–13. The selected superior features and corresponding frequency ranges are marked by shaded regions. Three different conditions, namely, the nominal model, control parameter $c_{sky} = 4000$ Ns/m, sprung mass $m_b = 500\,\text{kg}$ and $m_b = 300\,\text{kg}$, were compared.

Remark 5. Considering that the number of superior features is set as 4, the comparison in Figures 11, 12 and 13 only provides qualitative analysis from the frequency response perspective. In the time domain, since

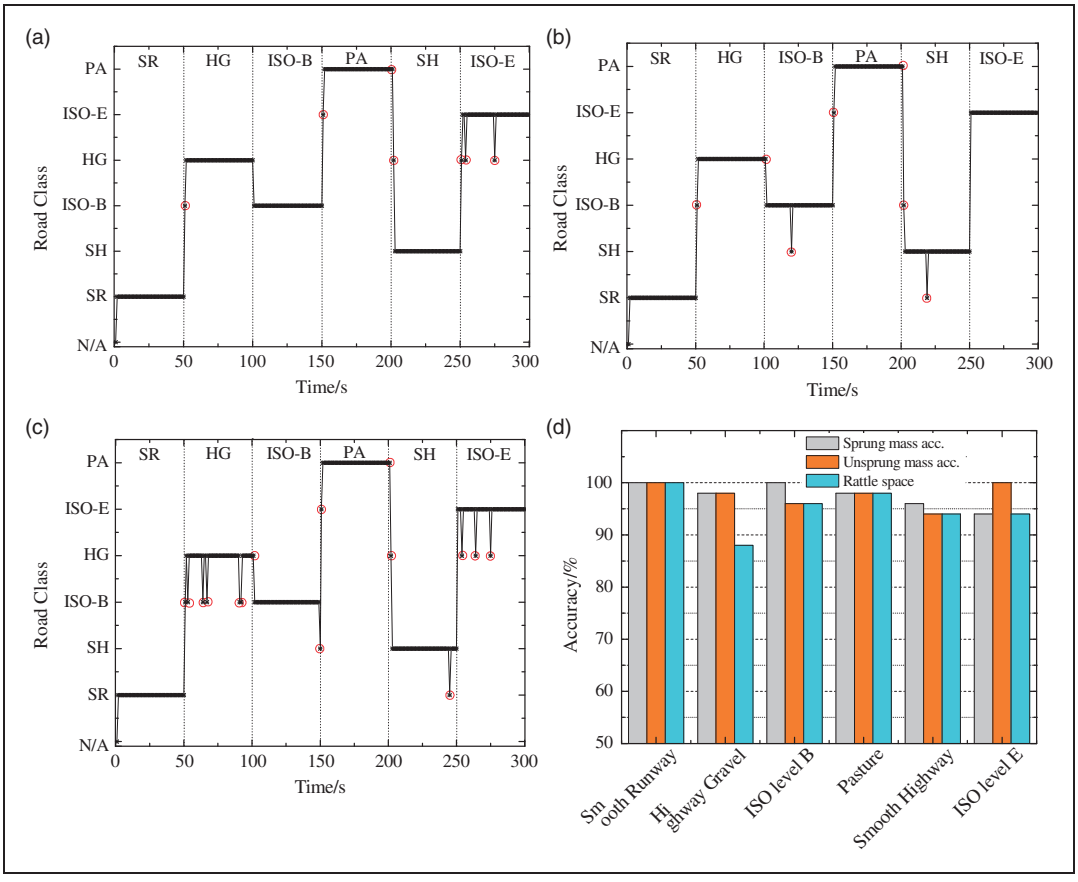

Figure 9. Classification results for $c_{sky} = 4000$ N s/m: (a) sprung mass acceleration, (b) unsprung mass acceleration, (c) rattle space, (d) classification accuracy.

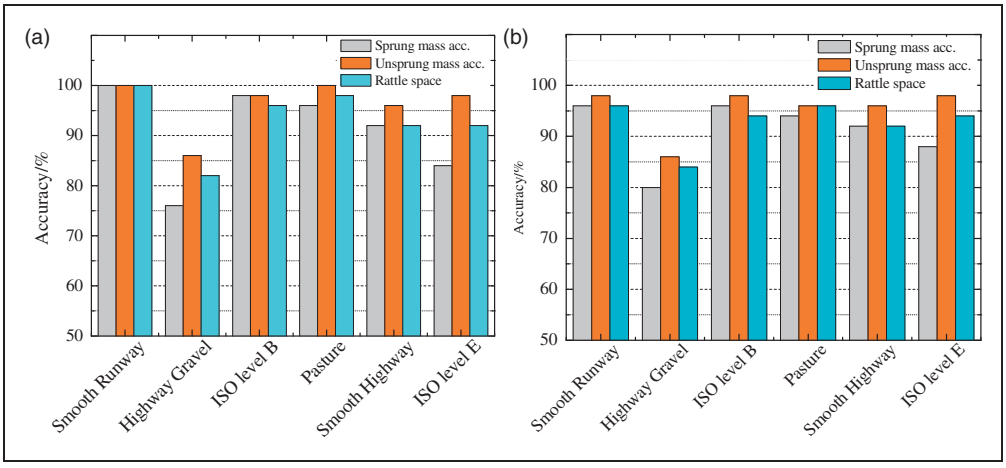

Figure 10. Classification results for varying sprung masses: (a) sprung mass of $m_b = 500$ kg, (b) sprung mass of $m_b = 300$ kg.

all superior features for the three sensors (except feature 4 of the unsprung mass acceleration, i.e. the maximum value of the time domain) can be described as the representation of the signal energy, and the area between the frequency response curve and axes can be interpreted as a statistical description of these time domain features.

As observed from the sprung mass acceleration response, two superior features are related to frequency components: SRA of aD2 (12.5 Hz ~ 25 Hz) and SRA

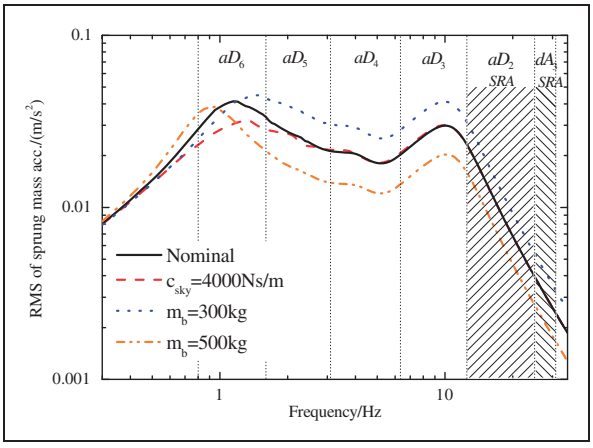

Figure 11. Frequency response of sprung mass acceleration. RMS: root mean square.

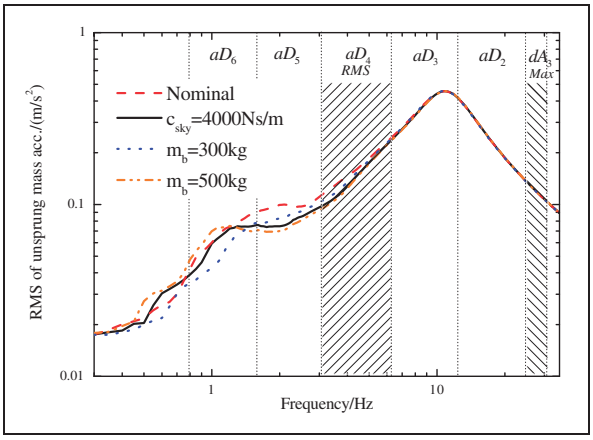

Figure 12. Frequency response of unsprung mass acceleration.

of dA3 (25 Hz ~ 31.3 Hz). For $c_{sky} = 4000$ N s/m, the response line (red dash) in the area of aD6 is depressed with a lower magnitude. In comparison, for both aD2 and dA3, the responses are almost the same. Thus, excellent robustness is shown with varying control parameters. When the driving condition changes to $m_b = 500$ kg and $m_b = 300$ k, the response difference is evident. The change of the sprung mass not only shifts the sprung mass resonance to the left ($m_b = 500$ kg) or right ($m_b = 300$ kg), but also depresses ($m_b = 500$ kg) or increases ($m_b = 300$ kg) the system response in the range of aD2 ~ aD5 and dA3. Such variations illustrate the serious deterioration of the sprung mass based classifier.

According to Figure 12, two superior features of the unsprung mass acceleration, RMS of aD4 (3.1 Hz ~ 6.3 Hz) and the maximum value of dA3 (25 Hz ~ 31.3 Hz), are chosen in the frequency domain. With the control parameter $c_{sky} = 4000$ N s/m, similar to the sprung mass acceleration, the changes in

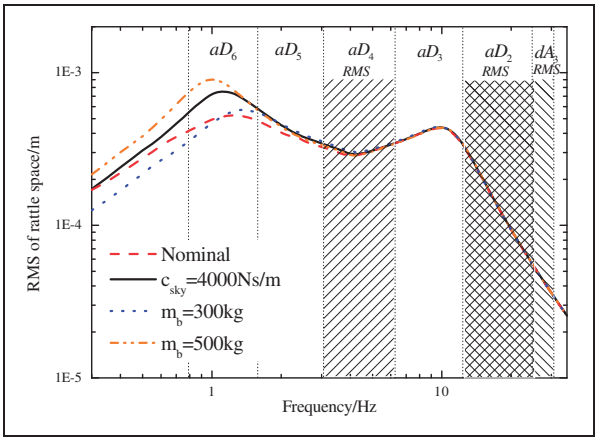

Figure 13. Frequency response of rattle space.

system response for both aD4 and dA3 are not obvious. This led to similar performance as the nominal model. For $m_b = 500$ kg and $m_b = 300$ kg, the variations of the unsprung mass acceleration response are relatively small in both aD4 and dA3, which led to little to no accuracy changes for the unsprung mass. Thus it can be concluded that the unsprung mass acceleration is more robust than the other two responses for varying controller parameters and the sprung mass.

Different from the sprung and unsprung mass acceleration, three features are selected as superior features for the system rattle space response: RMS of aD4 (3.1 Hz ~ 6.3 Hz), aD2 (12.5 Hz ~ 25 Hz) and dA3 (25 Hz ~ 31.3 Hz). Thus, the final classification results are mainly influenced by certain frequency ranges. For $c_{sky} = 4000$ N s/m, the system response differences in three frequency ranges are not obvious compared to the nominal model. This resulted in little to no changes in classification accuracy. When the sprung mass is $m_b = 500$ kg and $m_b = 300$ kg, similar results are obtained.

5.2.5. Comparison with existing methods. To better illustrate the properties of the proposed method, comparison with two existing methods is performed in this section. The first method of comparison is based on the back-propagation neural network (BPNN), and for more details, readers can refer to Ngwangwa et al. (2014). The second method of comparison is based on the Adaptive Neuro-Fuzzy Inference System (ANFIS), and for more details, readers can refer to Qin et al. (2015b). The reason why these two methods are selected is that the BPNN method represents a method where information comes from the time domain only, while the ANFIS method represents a method where information comes from both time and frequency domains with a distance based criterion for feature selection.

The unsprung mass acceleration is selected to represent the proposed methods. Since both output of BPNN and ANFIS methods are positive real numbers instead of integers, the classification accuracy is defined by checking whether the classified road level belongs to set A (assuming the correct output is y^*) (Qin et al., 2015b)

$$A = \left\{ y \in \Re^+ \,|\, y^* - 0.5 \le y \le y^* + 0.5, y^* = 1, 2, \cdots 6 \right\} \tag{20}$$

The comparison results for the nominal model, varying control parameters and sprung mass are shown in Figure 14.

Here, case 1 stands for the nominal model case, case 2 stands for the case of $c_{sky} = 4000$ N s/m, case 3 stands for the case of $m_b = 500$ kg, and case 4 stands for the case of $m_b = 500$ kg. It can be observed that the proposed method performed well in all three cases with estimation accuracy of more than 96%. For the BPNN method, more than 80% accuracy can be achieved for both case 1 and 2. However, when the sprung mass increases to 500 kg (decreased to 300 kg), the estimation accuracy decreases to 67% (70%). As for the ANFIS based method, although better performance than BPNN method can be observed, its performance is still worse than that of the proposed method. It can be concluded that the maximal relevance and minimum mutual redundancy criterion is more suitable than the distance based criterion for the road classification problem. According to the comparisons shown above, it can be concluded that the proposed method can outperform the BPNN and ANFIS based methods being more robust to various driving conditions.

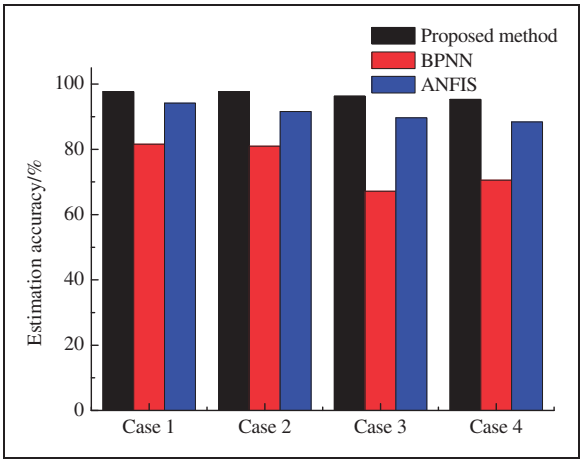

Figure 14. Comparison with BPNN and ANFIS based methods. BPNN: Back-propagation neural network; ANFIS: adaptive network-based fuzzy inference system (**ANFIS**).

5.2.6. Summary of numerical simulation. According to simulation results shown above, several conclusions regarding the proposed classifier can be made.

- From the perspective of the overall performance for each of the proposed classifiers, ranking from best to worst can be decided as unsprung mass acceleration performs, sprung mass acceleration and rattle space. Although the classification with the application of the sprung mass acceleration performed well with varying control parameters, the results reveal that the performance are highly sensitive to the value changes in the sprung mass. As for the unsprung mass acceleration based classifier, its performance can be ensured for both variation of controller parameters and $\pm 30\%$ change of the sprung mass, which is more than sufficient for mass production of vehicles.
- It can be seen from Figures 11, 12 and 13 that both a highway with gravel and ISO level E were susceptive to variations in driving conditions. According to Table 2, for these two levels, differences of adjacent levels are smaller compared to the other levels. Since, the normalization of different categories is performed in the training process of the PNN classifier, the relative distance of these two levels is smaller than the other levels, and lead to higher classification error rates. In this case, the candidate category choice is important, as the average distance chosen might be helpful in further improving system performance.
- For Figures 11, 12 and 13, the features in the frequency domain are located in regions larger than 3 Hz. This is due to the choice of the classification interval selected as 1 s. Statistical information on low-frequency components for each interval would always fluctuate, and it would be difficult to use it as a classification criterion. In this case, the mRMR abandons low-frequency components. To remedy this, the classification interval can be increased to introduce more low frequency components. However, for skyhook control applied in this paper, low frequency components, especially aD6, are sensitive to the variation of the control parameter and\or sprung mass. Moreover, if another control strategy is used to improve road handling, such as groundhook control, it may lead to a large variation in the high frequency range. In this case, the choice of the control interval should be made on a case-by-case basis relying on the operator judgment.

After obtaining the road level with the proposed method, the suspension control can be performed according to the identified road level. One widely accepted principle for suspension control has been proposed by Hong et al. (2002), and since this paper mainly focuses on providing a new classification algorithm,

regarding the question of how to adjust control parameters and design an observer with the identified road level and principles, readers can refer to Qin et al. (2015a) and Wang et al. (2016). It should also be noted that the road levels used in this paper are generated from Table 2. However, the actual road level may be located in between two adjacent levels. In this case, the classifier may output a classification result as either of these two levels, and the authors think that this output will not lead to a serious effect on the controller and observer's performance, since the road can be interpreted as either of the two levels.

6. Conclusion

In this paper, a novel method to classify road levels for a semi-active suspension system is introduced to solve problems associated with feature redundancy and robustness. The nonlinear QoV model and damping force characteristics are introduced, and six road levels with different PSD slopes are created for analysis. According to previous research results reported in literature, the SRA, RMS, variance and maximum value are selected as four basic statistical features. To improve the resolution within a certain frequency range, wavelet packet decomposition is utilized to decompose system response signals into six components. A total of 29 features are calculated to form a feature vector. In order to avoid dimensionality problems and data redundancy, the mRMR is used to select four superior features. With the selected features, the PNN classifier is used to identify the road class. Simulations are used to determine three measurable system responses for comparison, including the sprung mass acceleration, unsprung mass acceleration and rattle space. By varying control parameter c_{sky}, the sprung mass value and vehicle velocity, the robustness of the proposed method is demonstrated. According to the simulation results, the influence of the control parameter is negligible, increasing the sprung mass resulted in deterioration in accuracy of the sprung mass acceleration, and compared with existing methods, the proposed method with the application of the unsprung mass acceleration performs much better under all circumstances. It can thus be concluded from the results reported here that the classification with the unsprung mass acceleration demonstrated the best performance.

Further research is needed to investigate performance along the following aspects.

- The influence of different control strategies toward system response signals. The control strategy affects the system response, and this influence is reflected in the frequency domain. In this case, before features are imported into the mRMR, the features of frequencies that will be potentially influenced by the adaptive control strategy to improve system performance can be considered to be removed to improve classification accuracy.
- The proposed method provides a potential benefit for application of KF. An important step in the implementation of the KF is the determination of the process noise variance before estimation. In the case of suspension systems, the process noise is directly determined by the variance of road excitation. Many complex methods have been proposed in literature to estimate the variance (Xu et al., 2014; Pletschen et al., 2015) However, to the authors' best knowledge, little to no research has been presented in literature from the perspective of road estimation. The combination of the KF and the proposed method needs to be further studied.
- In this paper, the system response of only the nonlinear QoV model is investigated. When this method is applied to a whole vehicle, more information can be obtained with multiple sensors, and this new information can be applied to further improve the accuracy of prediction. Thus, the combination of information from different sensors and experiment validation will be performed in the near future.
- Assumption 3 restricts the investigated road profile to be stationary signals. However, there are numerous anomalies, such as ramps and speed bumps, that exist in actual roads. Further works will also focus on how to identify such anomalies and depress their influence on road classification.

Acknowledgments

The authors would also like to thank the editors and anonymous reviewers for their insightful comments and helping improve this paper.

Declaration of conflicting interests

The author(s) declared no potential conflicts of interest with respect to the research, authorship, and/or publication of this article.

Funding

The author(s) disclosed receipt of the following financial support for the research, authorship, and/or publication of this article: The authors acknowledge the support of the National Natural Science Foundation of China (grant number U1564210), Innovative talent support program for Chinese post doctorates (grant number BX201600017), and the China postdoctoral science foundation funded project (grant number 2016M600934).

References

Ahmed MM and Svaricek F (2014) Preview optimal control of vehicle semi-active suspension based on partitioning of

chassis acceleration and tire load spectra. In: *Control conference (ECC), 2014 European*, Strasbourg France, 25–27 June 2014, pp.1669–1674. IEEE.

BalaMurugan L and Jancirani J (2012) An investigation on semi-active suspension damper and control strategies for vehicle ride comfort and road holding. *Proceedings of the Institution of Mechanical Engineers, Part I: Journal of Systems and Control Engineering* 226: 1119-1129.

Cai Y, Huang T, Hu L, et al. (2012) Prediction of lysine ubiquitination with mRMR feature selection and analysis. *Amino Acids* 42: 1387–1395.

Deusen BDV (1968) Analytical techniques for designing riding quality into automotive vehicles. *SAE Transactions* 76, SAE paper No. 670021, DOI: 10.4271/670021.

Ding C and Peng H (2005) Minimum redundancy feature selection from microarray gene expression data. *Journal of Bioinformatics and Computational Biology* 3: 185–205.

Gonzalez A, O'brien EJ and Cashell K (2008) The use of vehicle acceleration measurements to estimate road roughness. *Vehicle System Dynamics* 46: 483–499.

Hong KS, Sohn HC and Hedrick JK (2002) Modified skyhook control of semi-active suspensions: A new model, gain scheduling, and hardware-in-the-loop tuning. *Journal of Dynamic Systems, Measurement, and Control* 124: 158–167.

Hrovat D (1997) Survey of advanced suspension developments and related optimal control applications. *Automatica* 33: 1781–1817.

Imine H, Delanne Y and M'Sirdi NK (2006) Road profile input estimation in vehicle dynamics simulation. *Vehicle System Dynamics* 44: 285–303.

ISO (1995) *Mechanical Vibration-Road Surface Profiles-Reporting of Measured Data*. Geneva, Swiss: International Organization for Standardization.

Jain AK, Duin RP and Mao J (2000) Statistical pattern recognition: A review. *IEEE Transactions on Pattern Analysis and Machine Intelligence* 22: 4–37.

Karnopp D, Crosby MJ and Harwood R (1974) Vibration control using semi-active force generators. *Journal of Engineering for Industry* 96: 619–626.

Koch G, Kloiber T and Lohmann B (2010) Nonlinear and filter based estimation for vehicle suspension control. In: *IEEE conference on decision and control*, Atlanta, GA, USA.

Liu H, Nonami K and Hagiwara T (2008) Active following fuzzy output feedback sliding mode control of real-vehicle semi-active suspensions. *Journal of Sound and Vibration* 314: 39–52.

McCann R and Nguyen S (2007) System identification for a model-based observer of a road roughness profiler. *IEEE region 5 technical conference,* Fayetteville, AR.

Martinez JC, Fergani S, Sename O, et al. (2015) Adaptive road profile estimation in semiactive car suspensions. *IEEE Transactions on Control Systems Technology* 23: 2293–2305.

Moustapha D, Alessandro V, Charara A, et al. (2011) Estimation of road profile for vehicle dynamics motion: experimental validation. In: *American control conference*, 29 June–1 July, San Francisco, CA, pp.5237–5242.

Ngwangwa HM, Heyns PS, Breytenbach HGA, et al. (2014) Reconstruction of road defects and road roughness classification using Artificial Neural Networks simulation and vehicle dynamic responses: Application to experimental data. *Journal of Terramechanics* 53: 1–18.

Nordberg TP (2004) An iterative approach to road profile identification utilizing wavelet parameterization. *Vehicle System Dynamics* 42: 413–432.

Peng H, Long F and Ding C (2005) Feature selection based on mutual information criteria of max-dependency, max-relevance, and min-redundancy. *IEEE Transactions on Pattern Analysis and Machine Intelligence* 27: 1226–1238.

Pletschen N, Barthelmes S and Boris L (2015) Joint state parameter estimation for active vehicle suspensions: A Takagi-Sugeno Kalman filtering approach. In: *IEEE conference on decision control*, 15–18 December, pp.1545–1550. Osaka, Japan.

Poussot VC, Spelta C, Sename O, et al. (2012) Survey and performance evaluation on some automotive semi-active suspension control methods: A comparative study on a single-corner model. *Annual Reviews in Control* 36: 148–160.

Qin YC (2016) *Research on vehicle semi-active suspension system based on road estimation*. PhD Thesis, Beijing Institute of Technology, China.

Qin YC, Dong M, Langari R, et al. (2015a) Adaptive hybrid control of vehicle semiactive suspension based on road profile estimation. *Shock and Vibration* 636739.

Qin YC, Dong MM, Zhao F, et al. (2015b) Road profile classification for vehicle semi-active suspension system based on adaptive neuro-fuzzy inference system. In: *IEEE control decision conference (CDC)*, 15–18 December, Osaka, Japan, pp.1533–1538.

Qin YC, Dong MM, Zhao F, et al. (2016) Comprehensive analysis for influence of controllable damper time delay on semi-active suspension control strategies. *Journal of Vibration and Acoustics Transactions of ASME* Accepted.

Qin YC, Guan JF and Gu L (2012) The research of road profile estimation based on acceleration measurement. *Applied Mechanics and Materials* 226-228: 1614–1617.

Qin YC, Reza L and Gu L (2014) The use of vehicle dynamic response to estimate road profile input in time domain. In: *ASME dynamic system control conference(DSCC)*, San Antonio, TX.

Rabhi A, M'sirdi NK, Fridman L, et al. (2006) Second order sliding mode observer for estimation of road profile. In: *Proceedings of the 2006 international workshop on variable structure systems*, Italy, 5–7 June, pp.161–165.

Rath JJ, Defoort M, Karimi HR, et al. (2016) Output feedback active suspension control with higher order terminal slding mode. *IEEE Transactions on Industrial Electronics*. Epub ahead of print 20 September 2016. DOI:10.1109/TIE.2016.2611587.

Sankaranarayanan V, Emekli ME, Gilvenc B, et al. (2008) Semiactive suspension control of a light commercial vehicle. *IEEE/ASME Transactions on Mechatronics* 13: 598–604.

Savaresi SM, Poussot VC, Cristiano S, et al. (2010) *Semi-active Suspension Control Design for Vehicles*. MA: Elsevier.

Specht DF (1990) Probabilistic neural networks. *Neural Networks* 3: 109–118.

Turnip A and Hong KS (2013) Road-frequency based optimization of damping coefficients for semi-active suspension systems. *International Journal of Vehicle Design* 63: 84–101.

Wang ZF, Dong MM, Qin YC, et al. (2016) Suspension system state estimation using adaptive Kalman filtering based on road classification. *Vehicle System Dynamics* Epub ahead of print 20 December 2016. DOI:10.1080/00423114.2016.1267374.

Wong J (2001) *Theory of Ground Vehicles*. New York, US: John Wiley & Sons.

Xu B, Zhang J and Guan X (2014) Estimation of the parameters of a railway vehicle suspension using model-based filters with uncertainties. *Proceedings of the Institution of Mechanical Engineers, Part F: Journal of Rail and Rapid Transit*. Epub ahead of print 12 February 2014. DOI:10.1177/0954409714521605.

Yi K and Song B (1999) A new adaptive sky-hook control of vehicle semi-active suspensions. *Proceedings of the Institution of Mechanical Engineers, Part D: Journal of Automobile Engineering* 213: 293–303.

Yu W, Zhang XJ, Guo KH, et al. (2013) Adaptive real-time estimation on road disturbances properties considering load variation via vehicle vertical dynamics. *Mathematical Problems in Engineering* 2013.

Zhang XJ, Yu WH, Ma FW, et al. (2012) Semi-active suspension adaptive control strategy based on hybrid control. In: *Proceedings of the FISITA 2012 world automotive congress*, Beijing, 27–30 November 2012, pp. 39–44.

Zhao F, Sam SZG, Tu FW, et al. (2016) Adaptive neural network control for active suspension system with actuator saturation. *IET Control Theory & Application* 14: 1696–1705.